Enhancing biochar redox properties through feedstock selection, metal preloading and post-pyrolysis treatments

Francisco J. Chacón [a,*]*, Miguel A. Sánchez-Monedero* [a]*, Luis Lezama* [b]*, M. Luz Cayuela* [a,**]

[a] Department of Soil and Water Conservation and Organic Waste Management, CEBAS-CSIC, PO Box. 164 Espinardo -30100 (Murcia-Spain)

[b] Departamento de Química Inorgánica, Facultad de Ciencia y Tecnología, Universidad del País Vasco, UPV/EHU, Apartado 644, 48080 (Bilbao-Spain)

Corresponding authors: *fjchacon@cebas.csic.es; **mlcayuela@cebas.csic.es

Abstract

There is growing evidence on the importance of the redox properties of biochar for many environmental applications. However, its variability and the difficulty in controlling its redox properties could be delaying the use of biochar in those areas that involve the exchange of electrons, like microbial fuel cells or contaminant degradation related to microbial electron shuttling. To help with these issues, we produced a wide range of biochars showing different redox capacities through a variety of strategies. These include optimizing production and processing parameters, feedstock selection, preloading biomass with redox-active metals and post-pyrolysis treatments. Modified Hummer's method was the most efficient treatment, increasing the electron donating capacity from 0.244 mmol e^-/$g_{biochar}$ to 0.590 mmol e^-/$g_{biochar}$ and the electron accepting capacity from 0.169 mmol e^-/$g_{biochar}$ to 0.645 mmol e^-/$g_{biochar}$. The
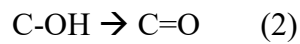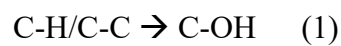
1

characterization of the phases responsible for the redox properties, mainly surface functional groups, radicals and redox-active metals, allowed us to better understand the changes caused to biochar by the different strategies. It revealed that the most important approach to enhance redox properties is to increase the number of C-OH and C=O groups in biochar, while the methods that use redox-active metals showed higher than predicted electron donating capacities. We also measured other attributes such as surface area, pH and conductivity, with a focus on their relationship with the redox properties. By selecting the appropriate production and modification methods, we were able to produce a balanced biochar with acceptable conductivity (1.34 mS/cm) and electron exchange capacity (0.418 mmol $e^-/g_{biochar}$), even though these properties usually have an inverse relationship. This work opens the possibility for the production of designer biochars with tailored properties optimized for specific applications.

Keywords: Biochar; Redox properties; Designer biochar; Functional groups; Conductivity.

1. Introduction

Traditional applications of biochar were mainly focused on carbon sequestration or improving soil physical properties and crop yields [1,2]. New research shows that the complex and heterogeneous nature of biochar can also have a role in many other activities, such as contaminant degradation, nutrient availability or microbial electron shuttling [3–7]. The redox properties of biochar have been proposed as an important factor in many of these environmental processes [8,9], as well as others related to areas such as microbial fuel cells and energy storage applications [10,11]. In biochar, these properties derive from the presence on its surface of certain functional groups, radicals and redox-active forms of metals like iron and manganese oxides [12,13]. In particular, phenolic C-OH moieties have been identified as the main groups

responsible for its electron donating capacity (EDC), while quinoid C=O moieties are behind its electron accepting capacity (EAC) [14]. Together, they determine the electron exchange capacity of the biochar (EEC, sum of EDC and EAC). Accordingly, enhancement of the redox properties would mainly require an increase in the quantity of these groups on the surface of biochar. Functionalization of the surface of carbonaceous materials most commonly involves an oxidation process [15]. The evolution of oxygen-containing functional groups after progressive oxidation tends to follow these steps:

$$C\text{-}H/C\text{-}C \rightarrow C\text{-}OH \quad (1)$$

$$C\text{-}OH \rightarrow C=O \quad (2)$$

$$C=O \rightarrow COOH \quad (3)$$

$$COOH \rightarrow CO_2 \quad (4)$$

Consequently, the oxidation process must be strong enough to introduce new functionalities, but not excessive to prevent their conversion to the redox-inactive COOH group or even removed as CO_2. This would also be important to avoid the oxidation of already existing redox-active functional groups in biochar.

Although radicals are usually short-lived, their presence in biochar as persistent free radicals (PFR) is high [16,17]. This is caused by the aromatic structure of biochar, which stabilizes by resonance the unpaired electrons, increasing their half-life from a few hours to months and even years [18,19]. Radicals influence the redox properties of biochar either as aryl radicals (carbon-centered) or as semiquinoid radicals (intermediate of the phenolic C-OH and quinoid C=O groups). Their high reactivity allows them to react with molecular oxygen to produce reactive oxygen species (ROS), which have been proved to catalyze different reactions, such as the degradation of contaminants in water [20,21]. Concerning the inorganic fraction of biochar, redox-active metals like Fe and Mn, commonly found in the feedstocks from which

biochar is produced, may appear in a range of oxidation states and can act both as electron donors and acceptors [22–24]. Their contribution to the electro exchange capacity will depend on the changes in speciation that these metals develop during pyrolysis and the resulting type and distributions of metal oxides and organo-mineral complexes on the surface [25]. Although the concentration of these metals is usually low on biochar, there has been some success in improving some of its properties by preloading the biomass material before and after pyrolysis [26–28].

Engineered/designer biochar has been used in the past to enhance some of its beneficial properties [29,30]. Although the pre-loading of biochar with metals and post-pyrolysis modifications have been reported in a range of articles, the majority of them did not consider the redox properties and instead focused on other properties like surface area, pH or cation exchange capacity. Only a few studies have tried to improve its redox properties [3,31,32]. However, they focused mostly on its electron donating capacity, which gives an incomplete view of its possibilities, specially given the potential reversibility of the electron exchange capacities [33]. Additionally, some applications may require biochars with specific redox properties (for example, a high electron accepting capacity), which is difficult to achieve due to the high variability of these properties between biochars [34,35]. This could have delayed the use of biochars with high redox capacities in many applications. A solution to these problems could be the controlled modification of biochar, with the objective of tailoring its redox properties for target applications. To fill this knowledge gap, we present the first systematic study that modifies a wide variety of biochars and measures their electron donating and accepting capacities.

The main objective was to produce biochars with a broad range of redox capacities to allow their use in specific applications. For this purpose, we altered biochar with different strategies,

including optimizing production and processing parameters, feedstock selection, preloading biomass with redox-active metals and post-pyrolysis treatments. To identify the components responsible for the changes in redox properties, we measured the variations in surface functional groups, radicals and redox-active metal content of the modified biochars. Since other biochar properties like surface area, pH and conductivity can also influence its effect on various applications, our secondary objective was to characterize them and when appropriate, establish their relationship with the redox properties.

2. Materials and methods

2.1. Chemicals

Iron (III) chloride (97%), nitric acid (70%), potassium hydroxide (>99%), potassium permanganate (99%), sodium chloride (>99.5%), sodium nitrate (>99%) and sodium phosphate monobasic (>99%) were purchased from Sigma-Aldrich. Sodium phosphate dibasic (>99%) was from Fluka. Hydrochloric acid (37%), hydrogen peroxide (30% w/v), phosphoric acid (88%), sodium hypochlorite (13%) and sulfuric acid (96%) were purchased from Panreac.

The electron transfer mediators 2,2′-azino-bis(3-ethylbenzothiazoline-6-sulfonic acid) diammonium salt (ABTS) (>98%) and neutral red (>90%) were from Sigma-Aldrich.

2.2. Feedstock preparation and characterization

A total of eight different plant feedstocks were used as starting materials: almond tree pruning (AlmondTP), carob tree pruning (CarobTP), giant reed (G_Reed), grapevine tree pruning (GrapevineTP), olive tree pruning (OliveTP), orange tree pruning (OrangeTP), rice husk (RiceH) and tomato plant (TomatoP). Raw materials were air dried, milled and sieved below 0.5 mm before analysis.

The elemental composition of C, H, and N was determined using an automatic elemental analyzer (LECO CHNS-932, USA). O content was calculated by difference, discounting ash content.

The lignin fraction was determined by the Klason method (ASTM D1106-96), cellulose by ASTM D1103-6 and hemicellulose concentration by subtracting the cellulose concentration from the delignified sample (hollocellulose) obtained by Browning's method.

2.3. Biochar production

Feedstocks were air dried, milled and sieved below 6 mm before pyrolysis. Biochar was produced via slow pyrolysis under Ar flux at different maximum temperatures (400, 600, 800 and 1000 ºC) in a RSR-B 80/500/11 rotatory tube furnace (Nabertherm, Germany). 0.5 L of feedstock was loaded into the tube and temperature ramps were programmed as follows: (1) linear heating at a rate of 5 ºC/min from room temperature to 105 ºC; (2) isotherm at 105ºC for 45 min; (3) linear heating at 5 ºC/min to the desired highest treatment temperature (HTT); (4) 2h of residence time at the HTT and (5) cooling down to ambient temperature. Biochars were ball milled for 30 seconds. To normalize particle size and allow comparison between biochars, particles of ground chars between 50 μm and 200 μm were selected via sieving before analysis and modification.

2.4. Biochar characterization

2.4.1. General physicochemical characterization

BET specific surface area and pore width were determined via N_2 adsorption/desorption isotherms obtained at 77.4 K in a Micromeritics ASAP 2020 system.

pH values were determined in a 1:20 (w/v) aqueous extract according to IBI [36].

XPS analysis was performed to obtain the surface atomic elemental composition and functional group distribution of the biochars using a K-Alpha X-ray XPS system (Thermo Scientific, UK) with a monochromatic Al Kα radiation source (energy 1486.68 eV) at 12 kV and 6 mA, and a spot size of 400 μm. The pass energy was of 200 eV to measure the whole energy band and 40 eV in a narrow scan with an energy step size of 1eV to selectively measure the selected elements. Charge compensation was achieved with a system flood gun. The quantitative analysis of XPS results was performed calculating the integral of each peak, where baselines were adjusted following the Shirley method. XPS spectra were processed with commercially available software (CasaXPS), and atomic concentrations were quantified by integration of the relevant photoelectron peaks. Assignment of peaks was based on literature [37]. Specifically, the C1s binding energies assigned were 284.4-284.6 eV and 285.0-285.2 eV for graphitic and aliphatic carbon, respectively, whereas 286.3-286.6 eV, 287.8-288.0 eV and 289.1-289.3 eV were assigned to hydroxyl (and ether), carbonyl and carboxyl functional groups, respectively.

The analysis of the conductive properties of the biochars was performed with a broadband dielectric spectrometer system (Novocontrol GmbH, Germany), providing a working frequency range from 0.1 Hz to 107 Hz. The measurement geometry was a disc shaped plate capacitor (20 mm diameter) where the specimen was placed between two gold plated brace electrodes. The thickness of the sample was 100 μm.

Metal concentration in biochars were measured after microwave HNO_3/H_2O_2 digestion by Inductively Coupled Plasma spectroscopy (ICP-OES) (ICAP 6500 DUO THERMO, Cheshire, UK).

For XRD analysis (Bruker D8 ADVANCE), samples were mounted as dry powders and scanned over the 10−100 º2θ range.

2.4.2. Radical content

Free radical content in biochars was determined by EPR using a Bruker ELEXSYS 500 spectrometer (X band) at room temperature. The spectrometer was equipped with a superhigh-Q resonator ER-4123-SHQ and the samples were placed in quartz tubes. The magnetic field was calibrated by a NMR probe and the frequency inside the cavity (~9.395 GHz) was determined with an integrated MW-frequency counter. Typical instrument settings were: center field, 3350 G; scan range, 200 G; receiver gain, 6.3×10^2; time constant, 40.96 ms; modulation amplitude, 1.0 G; modulation frequency 100 kHz; microwave power, 0.2 mW. The spin concentration (spins/gbiochar) was determined from the second integral of the recorded EPR spectrum and that of a known quantity of a standard sample of $CuSO_4 \cdot 5H_2O$. The data were collected and processed using the Bruker Xepr suite.

2.4.3. Electrochemical characterization

The electron exchange capacities were determined using a 3-electrode system following established methods [14,38]. The electron accepting capacity (EAC) and electron donating capacity (EDC) were normalized to the amount of biochar added and responsible for the electron exchange (mmol e$^-$/ g$_{biochar}$). The system consisted of a 20 mL glassy carbon crucible (Sigradur G, HTW, Germany) that acts both as a reaction vessel and working electrode, a Ag/AgCl reference electrode (Redoxme AB, Sweden) and a coiled platinum wire as an auxiliary electrode (Redoxme AB, Sweden), separated from the working electrode by a glass chamber with a porous frit. A 10 mM solution of 2,2′-azino- bis(3-ethylbenzthiazoline-6-sulfonic-acid) diammonium salt (ABTS) and 100 mM solution of neutral red (NR) were used as mediators for EDC and EAC, respectively. 15 ml of buffer solution (0.1 M NaCl, 0.1 M phosphate, pH 7) and 100 µL of mediator solution are added to the crucible and equilibrated to the desired redox potential (-0.49 V for EAC and +0.40 V for EDC, reported vs Ag/AgCl 3M KCl electrode). The integration of the reductive (EAC) and oxidative (EDC) current peaks

produced after the addition of 100 µL of biochar suspension (4 g/mL) allows calculating the electron exchange using Faraday's Law [9].

2.5. Biochar modification protocols

Olive tree pruning biochar produced at 400 ºC (OliveTP-B) was chosen as the control biochar for the following eight post-pyrolysis modifications: H_2O_2 [39], H_3PO_4 [40], HNO_3 [41], $KMnO_4$ [27], KOH [34], Modified Hummer's Method (MHM) [42], NaClO [43] and UV irradiation. The different protocols are briefly described in the Supporting Information (Text S1).

For the biochar exposed to air during pyrolysis (Air_ox-B), the purging gas line was removed during the cooling phase of a 400 ºC HTT pyrolysis of OliveTP at different temperatures of 350 ºC, 250 ºC and 150 ºC.

For the metal preloaded biochars, olive tree pruning biochar was preloaded with either Mn or Fe and then pyrolyzed at 400 ºC. Protocols are described in the Supporting Information (Text S2).

2.6. Treatment of data and statistics

The standard deviation of the electron exchange capacity (σ_{EEC}) was obtained from the variances and covariance of the electron donating (EDC) and accepting capacities (EAC), using the following formula:

$$\sigma_{EEC} = \sqrt{\sigma_{EDC}^2 + \sigma_{EAC}^2 + cov(EDC, EAC)}$$

Statistical analysis was conducted with Python, using the statsmodel and seaborn modules. Bootstrapping was used to calculate 95% confidence intervals. For linear regression, the t-test was used to estimate significance. For the quadratic fit, the F-test and t-test were used to obtain

the significance of the model and each individual regressor, respectively. Adjusted-R^2 was used here instead of R^2 to account for the additional variable.

3. Results and discussion

3.1. Influence of pyrolysis parameters, mechanical processing and aging

Pyrolysis conditions are key for the production of biochar with the desired redox properties, since they control the thermally induced changes caused to the original material [44]. The highest treatment temperature (HTT) is the most important parameter due to its influence on the type and concentration of functional groups on the surface of biochar [14]. To test its effect on the redox properties, olive tree pruning biomass (OliveTP) was pyrolyzed at different HTTs of 400 ºC, 600 ºC, 800 ºC and 1000 ºC. The highest electron exchange capacity (EEC) was found in the 400 ºC biochar, mainly due to the high number of C-OH moieties, and decreased as temperature rose (Fig. 1). Between 500-600 ºC, phenolic C-OH moieties are oxidized to quinoid C=O groups (Table S1), which explains the high electron accepting capacity (EAC) of the 600 ºC biochar. At higher temperatures, however, functional groups are removed from the surface of biochar and therefore its redox properties are greatly diminished.

Maintaining an inert atmosphere is essential for the pyrolysis process. Nevertheless, the addition of oxygen in the late stages of pyrolysis has been proposed in the past as a method for increasing the number of oxygen-containing functional groups (OCFGs) [45,46]. In order to examine this method, biochar was exposed to air by removing the purging gas line during the cooling phase of a 400 ºC HTT pyrolysis of Olive tree pruning. The exposure to air was started at different temperatures (350 ºC, 250 ºC and 150 ºC) to evaluate their effect on the oxidation of biochar. The yields of biochars obtained after pyrolysis and after exposure to air are shown in Table S2, with the 350 ºC exposure to air (Air_ox-B350) having the biggest mass loss (2.4%

higher loss with respect to the 31% yield of the original biochar). Biochar exposed to air at 150 ºC (Air_ox-B150) presented a small increase in EEC compared to the biochar produced under inert atmosphere (Fig. S1), mainly due to a higher EDC (electron donating capacity). This increase in electron donating capacity was in line with a higher concentration of C-OH
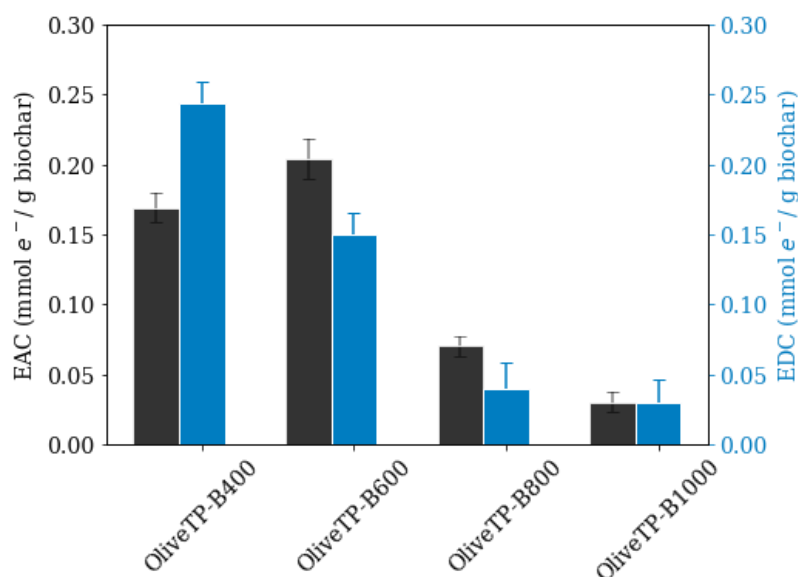

Fig. 1. Electron donating capacity (EDC, blue bars) and electron accepting capacity (EAC, black bars) of olive tree pruning biochar (OliveTP-B) pyrolyzed at different temperatures. Error bars represent 2 standard errors (n = 4 except OliveTP-B400 where n=5).

functional groups (Table S3), which suggests the introduction of new functionalities. In contrast, we found no significant differences in the EEC of the biochars exposed to air at 350 ºC and 250 ºC (and Air_ox-B250) compared to the biochar pyrolyzed under inert atmosphere. Despite this, they exhibited an increased EAC and decreased EDC, especially the biochar exposed at 350 ºC. XPS analysis (Fig. S2) explained the changes by showing a different surface functional group profile in these biochars, with a higher concentration of C=O and COOH groups at the expense of C-OH groups. This indicates a strong oxidation of the surface of biochar, which could have been excesive, leading to the removal of OCFGs as CO_2 and

offsetting the introduction of new functional groups. Further research could be done in this area by injecting controlled amounts of O_2 during pyrolysis.

Mechanical processing of biochar such as grinding or sieving is also expected to influence the redox properties of biochar, due to its effect on particle size and surface area [47]. Smaller particles generally have higher external surface area [48], which would expose more functional groups able to exchange electrons with the environment. We studied this effect by measuring the electron exchange capacity and surface area of an intact biochar (B-Intact) and comparing it with two other biochars, one ground by hand using a mortar and pestle (B-Mortar) and another by ball milling for 30 seconds (B-Ball_Mill) (Fig. S3, Table S4). As anticipated, the intact biochar had the lowest EEC and surface area. It also exhibited a very high variability between measures, which is probably a result of the heterogeinity in the shape and size of biochar fragments. Despite both ground biochars having a similar surface area, the ball milled biochar had a higher EEC compared to the mortar and pestle method. Although sometimes overlooked, these results show the importance of performing the appropriate mechanical processing to biochar depending on the desired application.
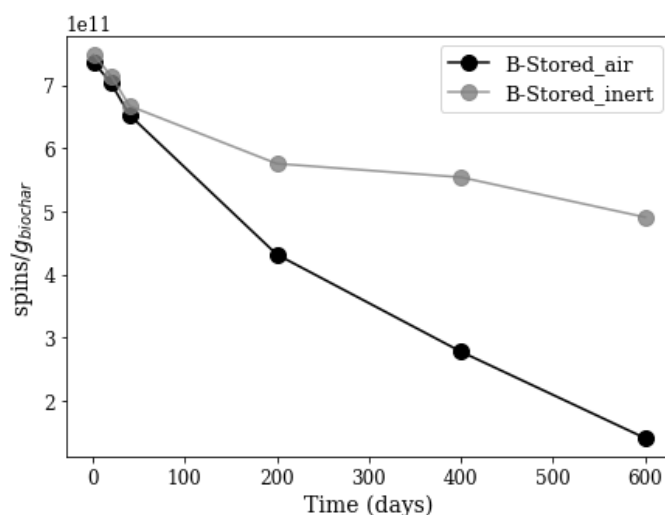

Fig. 2. Radical content of olive tree pruning biochar pyrolyzed at 400 ℃ and stored for 20 months (600 days) under inert atmosphere (B-Stored_inert) and exposed to air (B-Stored_air).

Storing conditions determine the changes induced by aging. We found no significant change in the redox properties of biochar after being stored for 20 months under an inert atmosphere (Fig. S4, Table S5). When the same biochar was exposed to air during storage, however, the result was higher redox capacities (especially EAC) and surface functionality. Radical content decreased with time, particularly in the biochar exposed to air, which showed five times less radicals than fresh biochar at the end of the 20 months (Fig. 2). Biological aging can also affect the redox properties of biochar with time. In a commercial biochar co-composted for 6 months [49] and stored for 18 months, the EEC increased only 12% compared to the original biochar (Table S6). However, the EAC was greatly reduced, while the EDC sharply increased. Previous research suggests that in addition to the oxidation of biochar, this could be derived from an organic coating on the surface of biochar formed during composting [50].

3.2. Influence of plant feedstock

To assess the influence of feedstock selection, we measured the surface functional groups and electron exchange capacity of eight biochars produced from different plant biomass at 400 ºC. Surface functional group profiles are similar for the different biochars, with the biggest changes found in the proportion of aliphatic C-C, C=O and COOH groups (Fig. 3A, Fig. S5). Comparing their redox capacities, the most remarkable are the high EDC of the tomato plant and grapevine tree pruning biochars, and especially the considerably high EAC of the orange tree pruning and rice husk biochars (Fig. 3B). The correlation between the concentration of surface C=O groups in these biochars and their EAC is much higher than between surface C-OH groups and EDC (Fig. 3C and 3D). This could indicate different ratios between the redox-active, aromatic forms of the functional groups (quinoid C=O and phenolic C-OH) and their
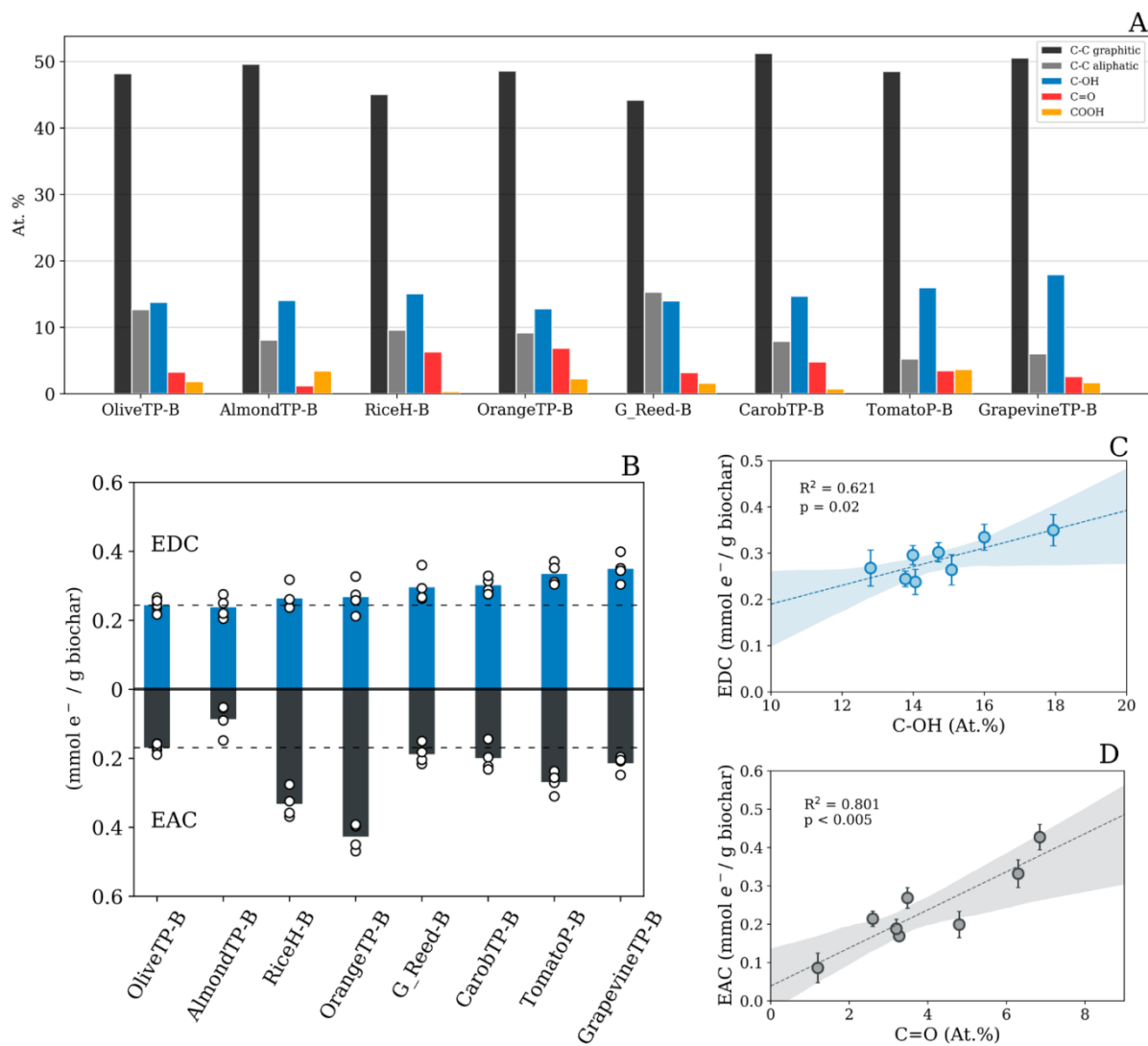
Fig. 3. (A) Atomic % concentration of graphitic carbon, aliphatic carbon, C-OH, C=O and COOH groups for biochars produced from different feedstocks. (B) Electron accepting capacity (EAC) and electron donating capacity (EDC) of the same biochars. Bars represent mean values. White dots are replicate measurements (n=4, except for OliveTP-B where n=5). (C) Correlation between the XPS measured atomic % of C-OH and EDC and (D) atomic % of C=O and EAC. Bands represent 95% confidence intervals for the linear fit. Error bars represent one standard deviation.

redox-inactive aliphatic counterparts (aliphatic C=O and C-OH groups). The difference between the aliphatic and aromatic form of the functional groups cannot be detected by XPS due to both forms having the same binding energies. The high correlation between EAC and C=O groups would represent a high relative amount of quinoid C=O to aliphatic C=O in these biochars, while the lower correlation between EDC and C-OH might indicate a more balanced ratio for the different forms of the C-OH group.

While there was no correlation between the H/C elemental ratio in these biochars and the electron exchange capacity, the O/C elemental ratio showed a quadratic relationship with the EEC (adj-R^2 = 0.720, significant at p=0.018) (Table S7, Fig. S6). However, no relationship was found between O/C nor H/C elemental ratios in the original feedstocks and the EEC of the resulting biochars (Table S8). Likewise, there was no correlation between the lignocellulosic fractions of the plant biomass and the redox capacities of biochars. Results suggest, however, a relationship between the ash content of the feedstocks and the EEC of biochars (Table S9, Fig. S7). This relationship is not linear, and instead follows a quadratic fit where the redox capacity increases with higher ash content until a certain level, after which the redox capacity starts to decrease (adj-R^2 = 0.774, significant at p=0.011). Metal ions from ashes have been proposed to favor depolymerization pathways during the thermal degradation of pyrolysis that promote the generation of functional groups [51,52]. At high ash concentration levels, however, this beneficial effect could be outweighed by the reduced C and O content.

We found no relationship between radical content and redox properties in the different biochars (Fig. S8), while the presence of redox-active metals was too low to have a meaningful effect (Table S10). This confirms previous research that suggested a dominating role of functional groups in establishing the redox properties of biochar [14]. Therefore, one of the primary targets for biochar modification methods should be the alteration of the surface functional group composition.

3.3. Preloading with redox-active metals

Metal preloading has been used in the past as a method to increase the number of functional groups on biochar [53,54]. The use of redox-active metals like Mn or Fe could be an interesting choice to enhance the redox properties of biochar [11]. To test this we preloaded biomass (OliveTP) with either Mn or Fe and then pyrolyzed it at 400 ºC. Both modified biochars demonstrated increased electron donating and accepting capacities (Fig. 4). While the percentage of C=O groups increased in proportion to the higher EAC, the fraction of C-OH groups decreased by 9% and 5% for the Fe and Mn preloaded biochars, respectively (Table S11), even though their EDC increased. Several reasons could explain the exceptionally high electron donation of the Mn- and Fe-preloaded biochars:
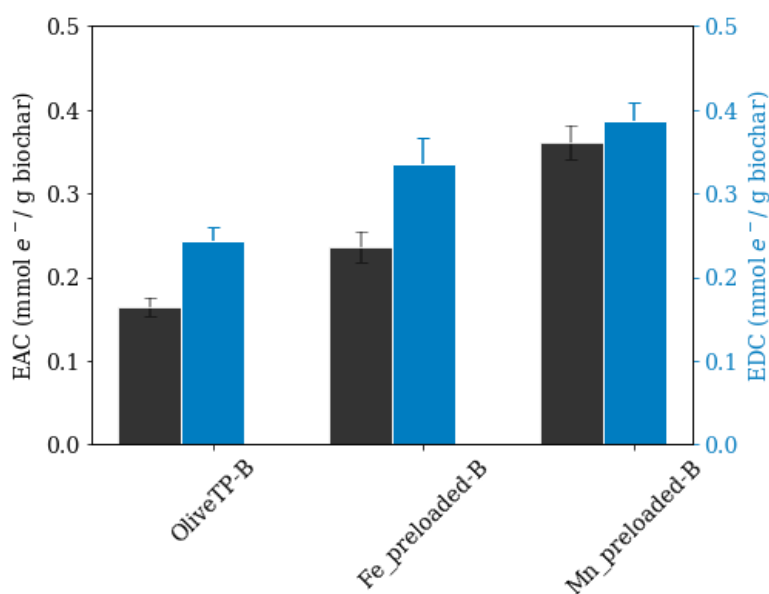

Fig. 4. Electron donating capacity (EDC, blue bars) and electron accepting capacity (EAC, black bars) of olive tree pruning biochar, Fe preloaded biochar and Mn preloaded biochar. Error bars represent 2 standard errors (n=4, except for OliveTP-B where n=5)

(i) The surface area of the biochars increased from 11.03 m^2/g in the control to 24.26 m^2/g in the Fe preloaded biochar and 43.11 m^2/g in the Mn preloaded biochar (Table 1). Previous research shows that Fe and Mn preloading can increase surface area through different mechanisms, including the formation of mineral structures on the surface [55,56] and the promotion of pore structures during pyrolysis [54,57]. This would expose more functional groups able to exchange electrons, which could remain hidden from the XPS analysis if the concentration of functional groups doesn't increase. In addition, if the new exposed areas are inside the pore structure they would remain undetected, since XPS is only able to measure the outer surface of biochar. It is important to highlight, however, that interpretation of BET results is limited for macroporous materials, which could be the case with these biochars.

(ii) Another explanation for the inflated EDC is an increase in the relative amount of phenolic C-OH to aliphatic C-OH. If the metal ions favor the formation of the redox-active form of C-OH in a higher ratio than the redox-inactive form, this could result in a lower but more electron donating C-OH fraction.

(iii) The surface atomic percentage of metals was 2% for Fe and 2.4% for Mn, while bulk concentrations were 6.34 w/w% and 5.36 w/w% for Fe preloaded and Mn preloaded biochar (Table S12). XRD analysis (Fig. S9 and S10) showed that the dominant crystalline mineral phases of Fe-preloaded and Mn-preloaded biochars were most probably magnetite and rancieite-type manganese oxides, respectively, both of which exhibit electrochemical capacity [58,59]. Therefore, in this case, appart from functional groups, there is a possible contribution of redox-active forms of metals to the electron exchange capacity.

3.4. Post-pyrolysis modification methods

Functional group profiles of the modified biochars show the deep changes in surface

chemistry that followed the different treatments (Fig. 5A, Fig. S11). This resulted in several of the modified biochars reaching much higher redox capacities than the biochars produced from different feedstocks (Fig. 5B). The most successful modification strategies were the $KMnO_4$ and Modified Hummer's method (MHM) treatments, which were able to double EDC and even triple the EAC of the original unmodified biochar. MHM is a method commonly used to produce graphite oxide and graphene oxide from graphite, which makes it suitable for the oxidation of another carbonaceous material like biochar. We skipped the sonication step in order to avoid the exfoliation of the biochar to graphene oxide and preserve some structural integrity. In this method, H_2SO_4 acts as an intercalation agent between aromatic sheets, opening the structure and producing a more efficient oxidation [60]. Accordingly, MHM was able to oxidize part of the graphitic fraction of biochar, achieving a more complete functionalization than other methods. Despite this, the increase in EDC of the MHM-modified biochar was only 13% higher than the $KMnO_4$- modified biochar, having a 32% higher density of C-OH groups. Additionally, even though

the proportion of C-OH functional groups was very similar in the HNO3 and KMnO4 treatments, the EDC was 53% higher in the latter. As in the Mn-preloaded biochar, the exceptionally high

EDC could be explained by the larger surface area (Table 1) or a higher proportion of redox-active C-OH groups than in the original biochar. XPS analysis indicated that only 1.1
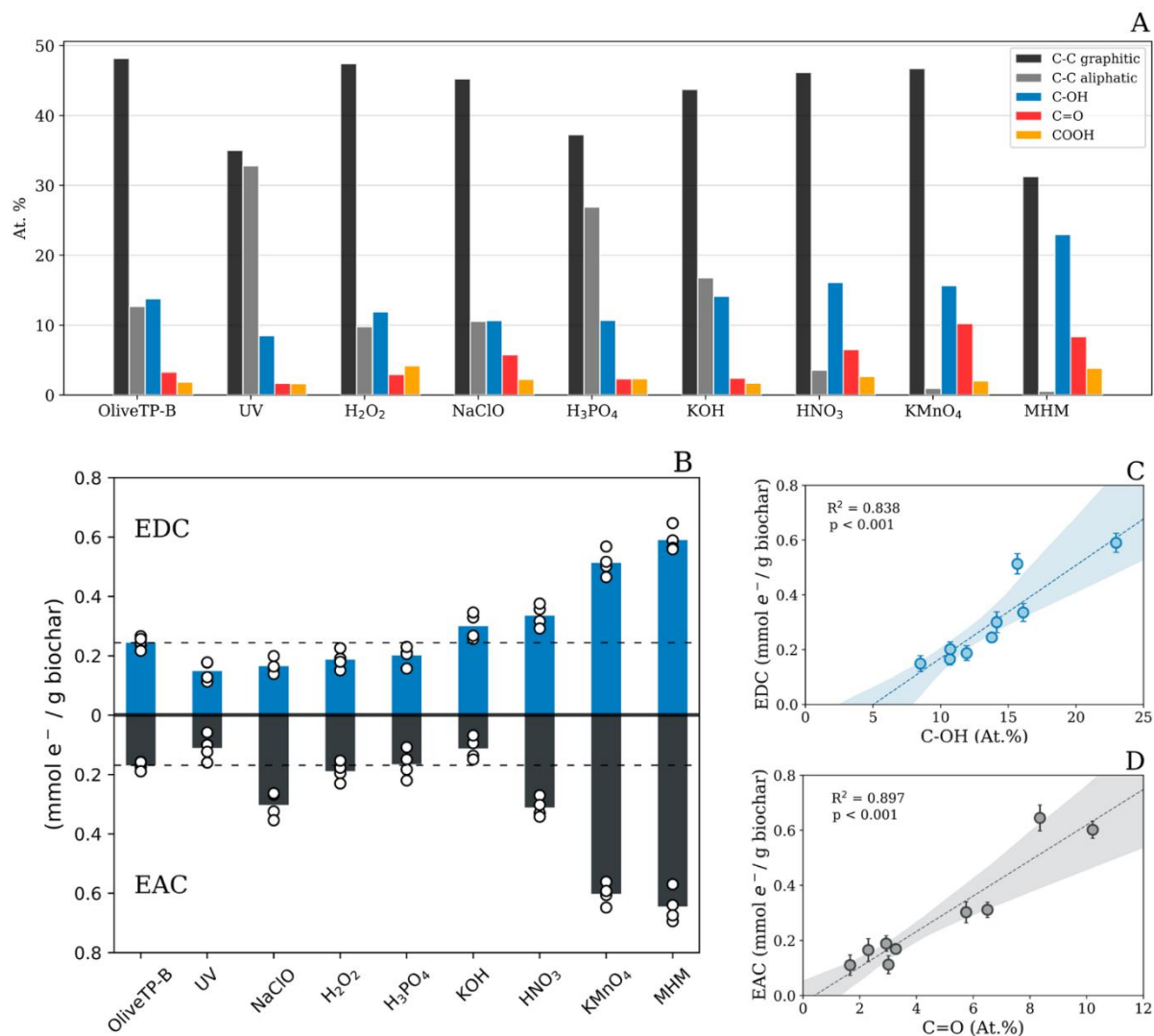
Fig. 5. (A) Atomic % values of graphitic carbon, aliphatic carbon, C-OH, C=O and COOH groups for the different biochars. (B) Electron accepting capacity (EAC) and electron donating capacity (EDC) of the untreated biochar (OliveTP-B) and the different modified biochars. Bars represent mean values. White dots are replicate measurements (n=5, except for OliveTP-B where n=5). (C) Correlation between the XPS measured atomic % of C-OH and EDC and (D) atomic % of C=O and EAC. Bands represent 95% confidence intervals for the linear fit. Error bars represent one standard deviation.

atomic % of Mn was present on the surface of the KMnO4-modified biochar, and the bulk Mn concentration was 0.21% w/w as measured by ICP-MS (Table S13). This is a much lower concentration of metal than in the Mn-preloaded biochar. Therefore, in this case the contribution of Mn to the redox capacity was probably weak.

Previous studies show that HNO_3 treatment on carbonaceous materials can introduce nitrogen groups on the surface [61], some of them redox-active. XPS analysis revealed that only a 2.6 atomic % of nitrogen was incorporated into the surface of the HNO_3-modified biochar, which is low compared to the proportion of oxygen-containing functional groups. Thus, the contribution of nitrogen-containing redox-active groups to the electrochemical properties of the HNO_3-modified biochar is likely small. Still, oxidation was able to increase EDC and EAC by 38% and 84%, respectively.

NaClO and KOH modification strategies, contrary to the previous treatments, did not increase both EAC and EDC simultaneously. NaClO added very few functional groups and mostly oxidized the existing C-OH groups to C=O, thus sacrificing EDC for EAC. KOH increased EDC at the expense of EAC. Since KOH is neither an oxidant nor a reducing agent, the change may be related to the increase in surface area (two-fold higher than the unmodified biochar).

H_2O_2 and H_3PO_4-modified biochars had a lower electron donating capacity than the original biochar. XPS analysis shows that H_2O_2 oxidation was excessive, converting a fraction of C-OH groups to the redox-inactive COOH. However, it could not generate sufficient new C-OH groups, resulting in the lower EDC. H_3PO_4 treatment was also not able to introduce new redox-active groups and only disrupted the integrity of the graphitic fraction of biochar, resulting in a very low surface area that may have reduced the redox properties even further.

For certain applications, a modification method that reduces the electron exchange capacity might be needed [62,63]. A green approach to reduce the number of functional groups and thus

the electron exchange capacity is UV irradiation under inert atmosphere. C-OH and C=O groups were removed from the surface and therefore both EDC and EAC were low. Moreover, the amount of functional group removal can be tuned by adjusting irradiation time (Fig. S12).

Table 1. N_2–BET surface area and pH values of the original and modified biochars.

	N_2–BET Surface area (m^2/g)	pH (1:20 w/v)
OliveTP-B	11.03	8.97
HNO_3	2.24	3.34
H_3PO_4	<2	6.3
H_2O_2	4.41	7.47
$KMnO_4$	124.28	7.55
KOH	24.50	10.10
MHM	3.16	3.3
NaClO	3.00	6.35
UV	8.67	9.34
Fe_preloaded-B	24.26	7.7
Mn_preloaded-B	43.11	8.76

The correlation between the proportion of C=O groups and EAC, and especially C-OH groups and EDC is much higher in the post-treatment biochars than in those produced from different feedstocks. (Fig. 5C and 5D). This is probably caused by a higher ratio of redox-active aromatic groups to redox-inactive aliphatic groups. The origin of the increased ratio could be either a favored addition of aromatic groups during oxidation or a lower stability of the aliphatic groups, that may have been removed during treatments. Radical content decreased in all treated biochars, but the decline was greater in the oxidative treatments, probably from the destruction of radicals during oxidation (Table S14).

One of the benefits of performing a wide variety of treatments is the possibility of modulating other indirect properties such as surface area, pH or conductivity. This can be important for identifying which factor is responsible for a specific effect on the environment or to design biochars with an optimized combination of tailored properties.

The already low surface area of the 400 ºC OliveTP-B (11.03 m^2/g) decreased even more for the majority of treatments, especially for the H_3PO_4-modified biochar, whose surface area and pore width was below quantification levels (Table 1). The exceptions were the KOH and $KMnO_4$ treatments,which increased surface area by 13.47 m^2/g and 113.25 m^2/g, respectively.

As expected, pH in a 1:20 w/v biochar suspension was related to the type of reagent used. Treatments with acids (HNO_3, H_3PO_4, MHM) decreased pH while KOH increased it. Oxidants also decreased pH, presumably related to the higher amount of C-OH and COOH functional groups. Inversely, UV irradiation raised the pH of the suspension, having a lower proportion of those functional groups.

3.5. General trend between redox properties and functional groups

Combining all previous functional group and redox properties data (except intact and mortar ground biochars) shows that the most important key element for enhanced redox properties is to increase the number of C-OH and C=O groups in biochar (Fig. 6). The exceptional electron donation capacity of the metal pre-loaded and $KMnO_4$-treated biochars stand out among the rest, achieving higher EDCs than predicted using only the content of C-OH functional groups. This confirms that methods that use redox-active metals (in our case, Fe and Mn) are among the most promising for enhanced redox properties.
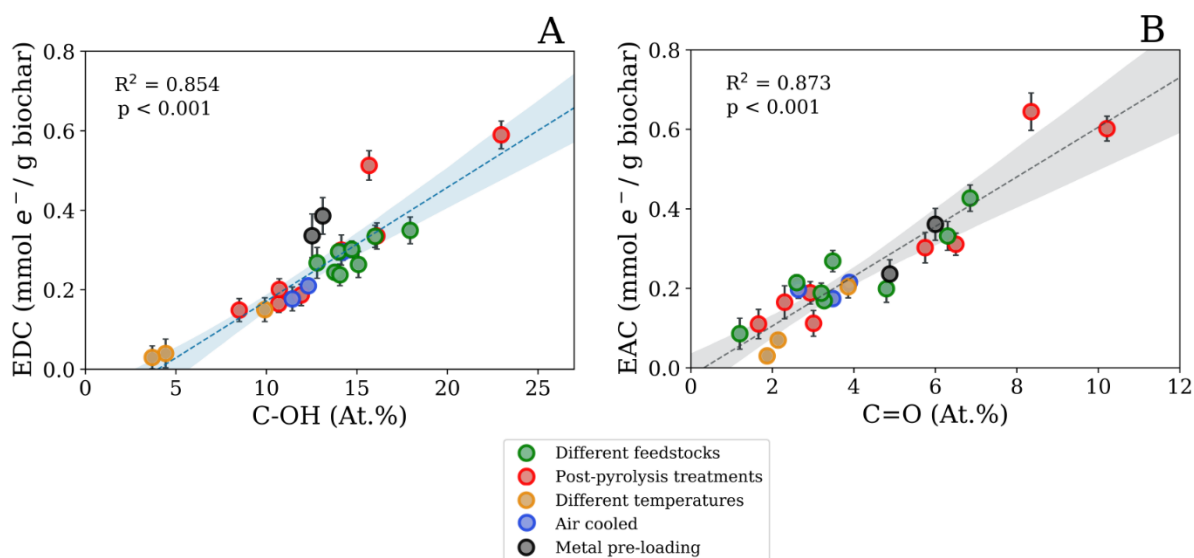
Fig. 6. (A) Correlation between the XPS measured atomic % of C-OH and EDC; and (B) atomic % of C=O and EAC for all previous biochars (except intact and mortar ground biochars). Bands represent 95% confidence intervals for the linear fit. Error bars represent one standard deviation.

3.6. Trade-offs between redox properties and conductivity

Some biochar applications require a combination of different properties to produce a significant effect [34]. One area where this happens is in processes that involve microbial electron shuttling, where many studies have reported the importance of both conductivity and redox properties for an optimal performance [64–66]. For example, in a recent work Prado et al. [67] used biochar as an electroconductive filter material that stimulated extracellular electron transfer and microbial degradation of wastewater. They found that although conductivity was a necessary component, redox-active functionalities on biochar increased considerably the electron transfer between the material and the microorganisms. This allowed for a more efficient biodegradation than other materials with higher conductivity but lower redox properties.
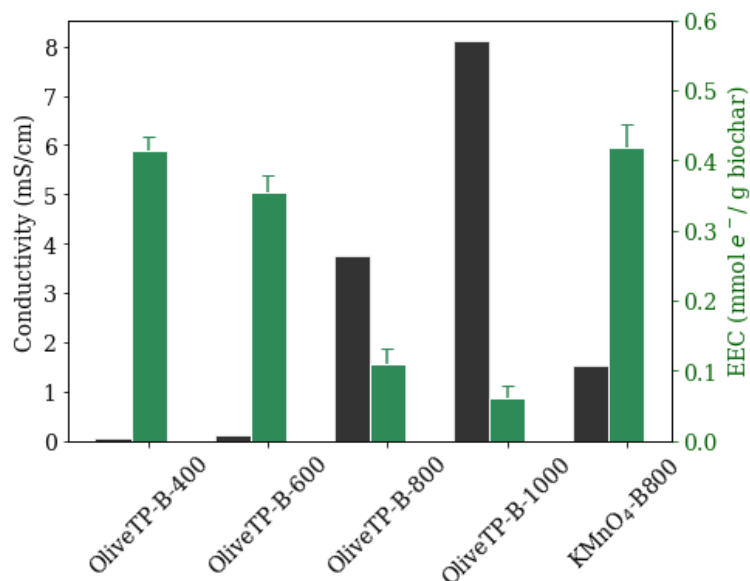
Fig. 7. Conductivity values (black bars, left axis) and EEC (green bars, right axis) of OliveTP biochar produced at different pyrolysis temperatures and a KMnO$_4$-modified biochar produced at 800 ºC. Error bars for EEC represent 2 standard errors (n = 4 except B-400 where n=5).

Conductivity increases with pyrolysis temperature due to growth and condensation of the amorphous carbon sheets, which end up forming a conductive network of graphite-like sheets that are able to transfer electrons between them [44,68]. To study its evolution with temperature, we pyrolyzed OliveTP biomass at increasing HTT (400, 600, 800 and 1000 ºC). Results showed that conductivity was negligible up until 800ºC, where it increased several orders of magnitude compared to lower temperature biochars (Fig. 7). At these high temperatures, however, the thermal degradation of functional groups drastically decreases the redox capacity of biochar. To increase the EEC, the KMnO$_4$-modification method was tested on the biochar pyrolyzed at 800 ºC (MHM was discarded due to the fragmentation of the graphitic structure caused by the intercalation step). Although the redox properties increased considerably, the conductivity of the modified biochar was greatly reduced. Previous research shows that the addition of functional groups tends to introduce defects on the the graphitic structure that provides conductivity to biochar, disrupting the electron transfer between

graphitic sheets [69]. Therefore, a compromise must be reached between conductivity and redox capacity. Despite this, the high temperature $KMnO_4$-modified biochar retained 40% of the conductivity of the untreated 800 ºC biochar, which was 25 times higher than the conductivity of biochar pyrolyzed at 400 ºC, while having a similar redox capacity. This balance between redox properties and conductivity could produce a greater effect in biochar applications that require both properties for an optimal performance.

4. Conclusions

In this work, we demonstrated the possibility of controlling the redox properties of biochar by modifying the nature and quantity of functional groups and redox-active metals on its surface. Moreover, other factors like surface area and pH can also be controlled by carefully choosing the type of modification strategy. Designer biochars with optimal property combinations can be produced this way to target specific applications or to identify the contribution of different properties in an experiment. For example, a biochar tailored for electron shuttling was created by controling the production temperature and post-pyrolysis modification with $KMnO_4$.

Declarations of interest: none

Appendix A. Supplementary material

Supplementary material associated with this article can be found at (no link provided yet).

References

[1]   L. Montanarella, E. Lugato, The Application of Biochar in the EU: Challenges and Opportunities, Agronomy. 3 (2013) 462–473. doi:10.3390/agronomy3020462.

[2]   J. Melorose, R. Perroy, S. Careas, Biochar for Environmental Management, 2015. doi:10.1017/CBO9781107415324.004.

[3]   K. Zhang, P. Sun, M.C.A.S. Faye, Y. Zhang, Characterization of biochar derived from rice husks and its potential in chlorobenzene degradation, Carbon N. Y. 130 (2018) 730–740. doi:10.1016/j.carbon.2018.01.036.

[4]   L. Kong, Y. Gao, Q. Zhou, X. Zhao, Z. Sun, Biochar accelerates PAHs biodegradation in petroleum-polluted soil by biostimulation strategy, J. Hazard. Mater. (2018). doi:10.1016/j.jhazmat.2017.09.040.

[5]   M.L. Cayuela, M.A. Sanchez-Monedero, A. Roig, K. Hanley, A. Enders, J. Lehmann, Biochar and denitrification in soils: when, how much and why does biochar reduce N(2)O emissions?, Sci. Rep. 3 (2013) 1732. doi:10.1038/srep01732.

[6]   B. Xiong, Y. Zhang, Y. Hou, H.P.H. Arp, B.J. Reid, C. Cai, Enhanced biodegradation of PAHs in historically contaminated soil by M. gilvum inoculated biochar, Elsevier Ltd, 2017. doi:10.1016/j.chemosphere.2017.05.020.

[7]   O. Husson, Redox potential (Eh) and pH as drivers of soil/plant/microorganism systems: A transdisciplinary overview pointing to integrative opportunities for agronomy, Plant Soil. 362 (2013) 389–417. doi:10.1007/s11104-012-1429-7.

[8]   Y. Yuan, N. Bolan, A. Prévoteau, M. Vithanage, J.K. Biswas, Y.S. Ok, H. Wang, Applications of biochar in redox-mediated reactions, Bioresour. Technol. 246 (2017) 271–281. doi:10.1016/j.biortech.2017.06.154.

[9]   Y. Xu, Y. Yan, N.L. Obadamudalige, Y.S. Ok, N. Bolan, Q. Li, Redox-Mediated Biochar-Contaminant Interactions in Soil, Elsevier Inc., 2019. doi:10.1016/B978-0-12-811729-3.00021-2.

[10]   Y. Yuan, T. Yuan, D. Wang, J. Tang, S. Zhou, Sewage sludge biochar as an efficient catalyst for oxygen reduction reaction in an microbial fuel cell, Bioresour. Technol. 144 (2013) 115–120. doi:10.1016/j.biortech.2013.06.075.

[11]   B.-H. Cheng, R.J. Zeng, H. Jiang, Recent developments of post-modification of biochar for electrochemical energy storage, Bioresour. Technol. (2017).

doi:10.1016/j.biortech.2017.07.060.

[12] F.J. Chacón, M.L. Cayuela, A. Roig, M.A. Sánchez-Monedero, Understanding, measuring and tuning the electrochemical properties of biochar for environmental applications, Rev. Environ. Sci. Bio/Technology. (2017). doi:10.1007/s11157-017-9450-1.

[13] S. Taherymoosavi, T. Thomas, S. Nielsen, J. Ye, G. Pan, C. Chia, S. Joseph, O. Husson, E. Graber, L. van Zwieten, S. Taherymoosavi, T. Thomas, S. Nielsen, J. Ye, G. Pan, C. Chia, P. Munroe, J. Allen, Y. Lin, X. Fan, S. Donne, The Electrochemical Properties of Biochars and How They Affect Soil Redox Properties and Processes, Agronomy. 5 (2015) 322–340. doi:10.3390/agronomy5030322.

[14] L. Klüpfel, M. Keiluweit, M. Kleber, M. Sander, Redox Properties of Plant Biomass-Derived Black Carbon (Biochar), (2014).

[15] W.J. Liu, H. Jiang, H.Q. Yu, Development of Biochar-Based Functional Materials: Toward a Sustainable Platform Carbon Material, Chem. Rev. 115 (2015) 12251–12285. doi:10.1021/acs.chemrev.5b00195.

[16] Y. Qin, G. Li, Y. Gao, L. Zhang, Y.S. Ok, T. An, Persistent free radicals in carbon-based materials on transformation of refractory organic contaminants (ROCs) in water: A critical review, Water Res. 137 (2018) 130–143. doi:10.1016/j.watres.2018.03.012.

[17] J. Yang, B. Pan, H. Li, S. Liao, D. Zhang, M. Wu, B. Xing, Degradation of p-Nitrophenol on Biochars: Role of Persistent Free Radicals, Environ. Sci. Technol. 50 (2016) 694–700. doi:10.1021/acs.est.5b04042.

[18] S. Liao, B. Pan, H. Li, D. Zhang, B. Xing, Detecting free radicals in biochars and determining their ability to inhibit the germination and growth of corn, wheat and rice seedlings, Environ. Sci. Technol. 48 (2014) 8581–8587. doi:10.1021/es404250a.

[19] G. Fang, C. Liu, J. Gao, D.D. Dionysiou, D. Zhou, Manipulation of persistent free radicals in biochar to activate persulfate for contaminant degradation, Environ. Sci. Technol. 49 (2015) 5645–5653. doi:10.1021/es5061512.

[20] G. Fang, J. Gao, C. Liu, D.D. Dionysiou, Y. Wang, D. Zhou, Key role of persistent free radicals in hydrogen peroxide activation by biochar: Implications to organic contaminant degradation, Environ. Sci. Technol. 48 (2014) 1902–1910. doi:10.1021/es4048126.

[21] G. Fang, C. Zhu, D.D. Dionysiou, J. Gao, D. Zhou, Mechanism of hydroxyl radical generation from biochar suspensions: Implications to diethyl phthalate degradation, Bioresour. Technol. 176 (2015) 210–217. doi:10.1016/j.biortech.2014.11.032.

[22] M. Sander, T.B. Hofstetter, C.A. Gorski, Electrochemical analyses of redox-active iron minerals: A review of nonmediated and mediated approaches, Environ. Sci. Technol. 49 (2015) 5862–5878. doi:10.1021/acs.est.5b00006.

[23] M. Risch, K.A. Stoerzinger, B. Han, T.Z. Regier, D. Peak, S.Y. Sayed, C. Wei, Z. Xu, Y. Shao-Horn, Redox Processes of Manganese Oxide in Catalyzing Oxygen Evolution and Reduction: An in Situ Soft X-ray Absorption Spectroscopy Study, J. Phys. Chem. C. 121 (2017) 17682–17692. doi:10.1021/acs.jpcc.7b05592.

[24] A. Dieguez-Alonso, A. Anca-Couce, V. Frišták, E. Moreno-Jiménez, M. Bacher, T.D. Bucheli, G. Cimò, P. Conte, N. Hagemann, A. Haller, I. Hilber, O. Husson, C.I. Kammann, N. Kienzl, J. Leifeld, T. Rosenau, G. Soja, H.P. Schmidt, Designing biochar properties through the blending of biomass feedstock with metals: Impact on oxyanions adsorption behavior, Chemosphere. (2019). doi:10.1016/j.chemosphere.2018.09.091.

[25] B.M. Reddy, Redox Properties of Metal Oxides, in: J.L.G. Fierro (Ed.), Met. Oxides Chem. Appl., Taylor & Francis, Boca Raton, 2006: pp. 215–246. doi:10.1002/chin.200610244.

[26] S. Wang, B. Gao, Y. Li, Y. Wan, A.E. Creamer, Sorption of arsenate onto magnetic iron–manganese (Fe–Mn) biochar composites, RSC Adv. 5 (2015) 67971–67978. doi:10.1039/C5RA12137J.

[27] M.C. Wang, G.D. Sheng, Y.P. Qiu, A novel manganese-oxide/biochar composite for efficient removal of lead(II) from aqueous solutions, Int. J. Environ. Sci. Technol. 12 (2015) 1719–1726. doi:10.1007/s13762-014-0538-7.

[28] B. Chen, Z. Chen, S. Lv, A novel magnetic biochar efficiently sorbs organic pollutants and phosphate, Bioresour. Technol. 102 (2011) 716–723. doi:10.1016/j.biortech.2010.08.067.

[29] A.U. Rajapaksha, S.S. Chen, D.C.W.W. Tsang, M. Zhang, M. Vithanage, S. Mandal, B. Gao, N.S. Bolan, Y.S. Ok, Engineered/designer biochar for contaminant removal/immobilization from soil and water: Potential and implication of biochar modification, Chemosphere. 148 (2016) 276–291. doi:10.1016/j.chemosphere.2016.01.043.

[30] B. Wang, B. Gao, J. Fang, Recent advances in engineered biochar productions and applications, Crit. Rev. Environ. Sci. Technol. 47 (2017) 2158–2207. doi:10.1080/10643389.2017.1418580.

[31] Y. Yan, X. Ma, W. Cao, X. Zhang, J. Zhou, Q. Liu, G. Qian, Identifying the reducing capacity of biomass derived hydrochar with different post-treatment methods, Sci. Total Environ. 643 (2018) 486–495. doi:10.1016/j.scitotenv.2018.06.232.

[32] S.Y. Oh, Y.D. Seo, K.S. Ryu, D.J. Park, S.H. Lee, Redox and catalytic properties of biochar-coated zero-valent iron for the removal of nitro explosives and halogenated phenols, Environ. Sci. Process. Impacts. 19 (2017) 711–719. doi:10.1039/c7em00035a.

[33] D. Xin, M. Xian, P.C. Chiu, New methods for assessing electron storage capacity and redox reversibility of biochar, Chemosphere. 215 (2019) 827–834. doi:10.1016/j.chemosphere.2018.10.080.

[34] C. Zhang, N. Zhang, Z. Xiao, Z. Li, D. Zhang, Characterization of biochars derived from different materials and their effects on microbial dechlorination of pentachlorophenol in a consortium, RSC Adv. 9 (2019) 917–923. doi:10.1039/C8RA09410A.

[35] Y. Zhang, X. Xu, L. Cao, Y.S. Ok, X. Cao, Characterization and quantification of electron donating capacity and its structure dependence in biochar derived from three waste biomasses, Chemosphere. 211 (2018) 1073–1081.

doi:10.1016/j.chemosphere.2018.08.033.

[36]   IBI, Standardized product definition and product testing guidelines for biochar that is used in soil, v. 1.1, Int. Biochar Initiat. (2015) 1–47. doi:http://www.biochar-international.org/characterizationstandard. 22.

[37]   F.R. Amin, Y. Huang, Y. He, R. Zhang, G. Liu, C. Chen, Biochar applications and modern techniques for characterization, Clean Technol. Environ. Policy. (2016). doi:10.1007/s10098-016-1218-8.

[38]   A. Prévoteau, F. Ronsse, I. Cid, P. Boeckx, K. Rabaey, The electron donating capacity of biochar is dramatically underestimated, Sci. Rep. 6 (2016) 32870. doi:10.1038/srep32870.

[39]   Y. Xue, B. Gao, Y. Yao, M. Inyang, M. Zhang, A.R. Zimmerman, K.S. Ro, Hydrogen peroxide modification enhances the ability of biochar (hydrochar) produced from hydrothermal carbonization of peanut hull to remove aqueous heavy metals: Batch and column tests, Chem. Eng. J. 200–202 (2012) 673–680. doi:10.1016/j.cej.2012.06.116.

[40]   Y. Lin, P. Munroe, S. Joseph, R. Henderson, A. Ziolkowski, Water extractable organic carbon in untreated and chemical treated biochars, Chemosphere. 87 (2012) 151–157. doi:10.1016/j.chemosphere.2011.12.007.

[41]   F. Güzel, H. Sayğılı, G. Akkaya Sayğılı, F. Koyuncu, C. Yılmaz, Optimal oxidation with nitric acid of biochar derived from pyrolysis of weeds and its application in removal of hazardous dye methylene blue from aqueous solution, J. Clean. Prod. 144 (2017) 260–265. doi:10.1016/j.jclepro.2017.01.029.

[42]   A.H. Lima, J.P. Mendonça, M. Duarte, F. Stavale, C. Legnani, G.S.G. De Carvalho, I.O. Maciel, F. Sato, B. Fragneaud, W.G. Quirino, Reduced graphene oxide prepared at low temperature thermal treatment as transparent conductors for organic electronic applications, Org. Electron. 49 (2017) 165–173. doi:10.1016/j.orgel.2017.05.054.

[43]   J. Wenk, M. Aeschbacher, E. Salhi, S. Canonica, U. Von Gunten, M. Sander, Chemical Oxidation of Dissolved Organic Matter by Chlorine Dioxide, Chlorine, And Ozone: E ff ects on Its Optical and Antioxidant Properties, Environ. Sci. Technol. 47 (2013) 11147–11156. doi:10.1021/es402516b.

[44]   M. Keiluweit, P.S. Nico, M.G. Johnson, Dynamic Molecular Structure of Plant Biomass-Derived Black Carbon (Biochar), 44 (2010) 1247–1253.

[45]   J.W. Lee, A.C. Buchanan, B.R. Evans, M. Kidder, Oxygenation of biochar for enhanced cation exchange capacity, in: Adv. Biofuels Bioprod., 2013. doi:10.1007/978-1-4614-3348-4_4.

[46]   W. Suliman, J.B. Harsh, N.I. Abu-Lail, A.M. Fortuna, I. Dallmeyer, M. Garcia-Perez, Modification of biochar surface by air oxidation: Role of pyrolysis temperature, Biomass and Bioenergy. 85 (2016) 1–11. doi:10.1016/j.biombioe.2015.11.030.

[47]   W. Liao, S. Thomas, Biochar Particle Size and Post-Pyrolysis Mechanical Processing Affect Soil pH, Water Retention Capacity, and Plant Performance, Soil Syst. 3 (2019) 14. doi:10.3390/soilsystems3010014.

[48]   A. Manikandan, Effect of High Energy Ball Milling on Particle Size and Surface Area

of Adsorbents for Efficient Loading of Fertilizer, An Asian J. Soil …. 8 (2011) 2013. http://www.researchjournal.co.in/online/AJSS/AJSS 8(2)/8_249-254_A.pdf.

[49] I. López-Cano, A. Roig, M.L. Cayuela, J.A. Alburquerque, M.A. Sánchez-Monedero, Biochar improves N cycling during composting of olive mill wastes and sheep manure, Waste Manag. 49 (2016) 553–559. doi:10.1016/j.wasman.2015.12.031.

[50] N. Hagemann, S. Joseph, H.-P.P. Schmidt, C.I. Kammann, J. Harter, T. Borch, R.B. Young, K. Varga, S. Taherymoosavi, K.W. Elliott, A. McKenna, M. Albu, C. Mayrhofer, M. Obst, P. Conte, A. Dieguez-Alonso, S. Orsetti, E. Subdiaga, S. Behrens, A. Kappler, Organic coating on biochar explains its nutrient retention and stimulation of soil fertility, Nat. Commun. 8 (2017) 1–11. doi:10.1038/s41467-017-01123-0.

[51] O.R. Harvey, B.E. Herbert, L.J. Kuo, P. Louchouarn, Generalized two-dimensional perturbation correlation infrared spectroscopy reveals mechanisms for the development of surface charge and recalcitrance in plant-derived biochars, Environ. Sci. Technol. 46 (2012) 10641–10650. doi:10.1021/es302971d.

[52] N. Shimada, H. Kawamoto, S. Saka, Different action of alkali/alkaline earth metal chlorides on cellulose pyrolysis, J. Anal. Appl. Pyrolysis. 81 (2008) 80–87. doi:10.1016/j.jaap.2007.09.005.

[53] H. Wang, B. Gao, S. Wang, J. Fang, Y. Xue, K. Yang, Removal of Pb(II), Cu(II), and Cd(II) from aqueous solutions by biochar derived from KMnO4 treated hickory wood, Bioresour. Technol. 197 (2015) 356–362. doi:10.1016/j.biortech.2015.08.132.

[54] W.-J. Liu, K. Tian, H. Jiang, H.-Q. Yu, Facile synthesis of highly efficient and recyclable magnetic solid acid from biomass waste., Sci. Rep. 3 (2013) 2419. doi:10.1038/srep02419.

[55] L. Zhou, Y. Huang, W. Qiu, Z. Sun, Z. Liu, Z. Song, Adsorption Properties of Nano-MnO2–Biochar Composites for Copper in Aqueous Solution, Molecules. 22 (2017) 173. doi:10.3390/molecules22010173.

[56] G. Akgül, T.B. Maden, E. Diaz, E.M. Jiménez, Modification of tea biochar with Mg, Fe, Mn and Al salts for efficient sorption of PO43− and Cd2+ from aqueous solutions, J. Water Reuse Desalin. 9 (2018) 57–66. doi:10.2166/wrd.2018.018.

[57] S. Wang, B. Gao, Y. Li, A. Mosa, A.R. Zimmerman, L.Q. Ma, W.G. Harris, K.W. Migliaccio, Manganese oxide-modified biochars: Preparation, characterization, and sorption of arsenate and lead, Bioresour. Technol. 181 (2015) 13–17. doi:10.1016/j.biortech.2015.01.044.

[58] S.G. Woo, H. Kim, C.K. Lee, H.J. Sohn, T. Kang, Electrochemical characteristics of rancieite-type manganese oxide by mechanochemical synthesis, J. Power Sources. 124 (2003) 174–181. doi:10.1016/S0378-7753(03)00619-0.

[59] P. Tipsawat, U. Wongpratat, S. Phumying, N. Chanlek, K. Chokprasombat, S. Maensiri, Magnetite (Fe 3 O 4) nanoparticles: Synthesis, characterization and electrochemical properties, Appl. Surf. Sci. 446 (2018) 287–292. doi:10.1016/j.apsusc.2017.11.053.

[60] Y.L. Zhong, Z. Tian, G.P. Simon, D. Li, Scalable production of graphene via wet chemistry: Progress and challenges, Mater. Today. 18 (2015) 73–78. doi:10.1016/j.mattod.2014.08.019.

[61] J.W. Lang, X. Bin Yan, W.W. Liu, R.T. Wang, Q.J. Xue, Influence of nitric acid modification of ordered mesoporous carbon materials on their capacitive performances in different aqueous electrolytes, J. Power Sources. 204 (2012) 220–229. doi:10.1016/j.jpowsour.2011.12.044.

[62] H. Yuan, Z. Zhang, M. Li, T. Clough, N. Wrage-Mönnig, S. Qin, T. Ge, H. Liao, S. Zhou, Biochar's role as an electron shuttle for mediating soil N2O emissions, Soil Biol. Biochem. 133 (2019) 94–96. doi:10.1016/J.SOILBIO.2019.03.002.

[63] G. Choppala, N. Bolan, A. Kunhikrishnan, R. Bush, Differential effect of biochar upon reduction-induced mobility and bioavailability of arsenate and chromate, Chemosphere. 144 (2016) 374–381. doi:10.1016/j.chemosphere.2015.08.043.

[64] G. Chen, Z.Z. Zhang, Z.Z. Zhang, R. Zhang, Redox-active reactions in denitrification provided by biochars pyrolyzed at different temperatures, Sci. Total Environ. 615 (2017) 1547–1556. doi:10.1016/j.scitotenv.2017.09.125.

[65] L. Yu, Y. Yuan, J. Tang, Y. Wang, S. Zhou, Biochar as an electron shuttle for reductive dechlorination of pentachlorophenol by Geobacter sulfurreducens, Sci. Rep. 5 (2015) 16221. doi:10.1038/srep16221.

[66] W. Tan, L. Wang, H. Yu, H. Zhang, X. Zhang, Y. Jia, T. Li, Q. Dang, D. Cui, B. Xi, Accelerated Microbial Reduction of Azo Dye by Using Biochar from Iron-Rich-Biomass Pyrolysis, Materials (Basel). 12 (2019) 1079. doi:10.3390/ma12071079.

[67] A. Prado, R. Berenguer, A. Esteve-Núñez, A.E.-N. Amanda Prado, Raúl Berenguer, Electroactive biochar outperforms highly conductive carbon materials for biodegrading pollutants by enhancing microbial extracellular electron transfer, Carbon N. Y. 146 (2019) 597–609. doi:10.1016/j.carbon.2019.02.038.

[68] A.G. Pandolfo, A.F. Hollenkamp, Carbon properties and their role in supercapacitors, J. Power Sources. 157 (2006) 11–27. doi:10.1016/j.jpowsour.2006.02.065.

[69] S.S. Barton, J.E. Koresh, A study of the surface oxides on carbon cloth by electrical conductivity, Carbon N. Y. 22 (1984) 481–485. doi:10.1016/0008-6223(84)90079-4.

Graphical abstract